Efficient quantum dot single photon extraction into an optical fiber using a nanophotonic directional coupler

M. Davanço,[1,2,*] M. T. Rakher,[1] W. Wegscheider,[3] D. Schuh,[3] A. Badolato,[4] and K. Srinivasan[1]

[1] *Center for Nanoscale Science and Technology, National Institute of Standards and Technology, Gaithersburg, MD 20899, USA*
[2] *Maryland NanoCenter, University of Maryland, College Park, MD 20742, USA*
[3] *Institute for Experimental and Applied Physics, University of Regensburg, D-93053 Regensburg, Germany*
[4] *Department of Physics and Astronomy, University of Rochester, Rochester, New York 14627, USA*

We demonstrate a spectrally broadband and efficient technique for collecting emission from a single InAs quantum dot directly into a standard single mode optical fiber. In this approach, an optical fiber taper waveguide is placed in contact with a suspended GaAs nanophotonic waveguide with embedded quantum dots, forming a broadband directional coupler with standard optical fiber input and output. Efficient photoluminescence collection over a wavelength range of tens of nanometers is demonstrated, and a maximum collection efficiency of 6 % (corresponding single photon rate of 3.0 MHz) into a single mode optical fiber is estimated for a single quantum dot exciton.

Single epitaxially grown quantum dots (QDs) can serve as bright, stable sources of single photons for applications in quantum information processing [1]. A key limitation of QDs embedded in high refractive index semiconductors is the relatively small fraction of the total QD emission ($\approx$ 1 %) [2, 3] that can be collected in free-space by a high numerical aperture optic, a consequence of total internal reflection at the semiconductor-air interface. Embedding the QD in a high quality factor (Q), small mode volume resonator such as a micropillar cavity [4, 5] is one approach to improving photon extraction, where ideally one benefits from both a faster radiative rate (Purcell enhancement) and a far-field emission pattern that can be efficiently collected. High extraction efficiencies have indeed been demonstrated with this approach [6]. One challenging aspect of using a high-Q microcavity is the necessity for spectral overlap between a narrow cavity mode and the QD emission line, though tunable geometries [7] can overcome this challenge. Alternatively, spectrally broadband approaches (usually without Purcell enhancement) avoid precise tuning and are needed for efficient spectroscopy of multiple spectrally distinct QD transitions and/or emission from multiple QDs, and have recently been pursued using solid immersion lenses [8, 9] and in vertically oriented tapered nanowire geometries [10]. Here, we demonstrate a guided wave nanophotonic structure for efficient extraction of PL from a single InAs QD directly into an optical fiber, with an operation bandwidth of tens of nm, and an overall single mode fiber collection efficiency of $\approx$6 %. Since collection is directly into an optical fiber, optical losses associated with light extraction using a typical microphotoluminescence setup and coupling from free-space into an optical fiber are completely avoided. Furthermore, this geometry is planar, avoiding deeply etched, vertically-oriented geometries, and could serve as a platform for waveguide-based photonic circuits involving single QDs and efficient coupling to optical fibers.

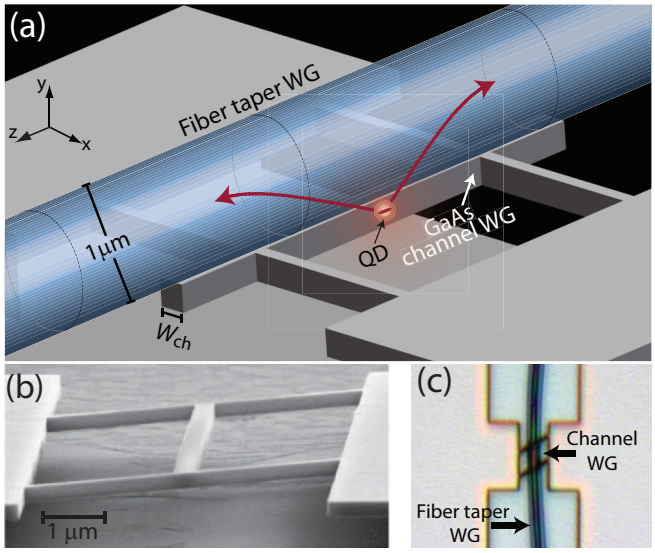

FIG. 1: (a) Nanophotonic directional coupler for single photon extraction from a single embedded QD. (b) SEM image of a fabricated GaAs channel WG. (c) Optical microscope image of the FTW/channel WG directional coupler.

Our structure is a hybrid directional coupler formed by a suspended GaAs channel waveguide (WG) containing InAs QDs and a micron diameter optical fiber taper waveguide (FTW) (Fig. 1(a)). The FTW is an optical fiber whose diameter is adiabatically reduced to a wavelength scale minimum, providing access to an evanescent field for guided wave coupling while maintaining single mode fiber ends and low loss. The GaAs WG (Fig. 1(b)) has a cross-sectional diameter of $\approx$ 100 nm, enabling phase matching to the FTW and efficient power transfer between the two WGs [11]. This structure supports single guided modes with strong transverse confinement, into which QD radiation is almost completely coupled. Efficient QD coupling to WG modes phase-matched to the

*Electronic address: mdavanco@nist.gov

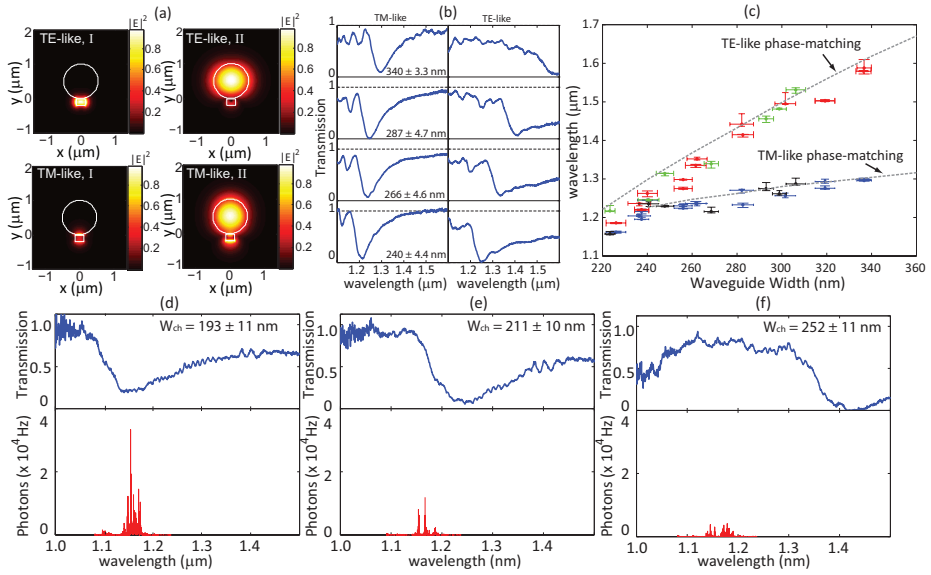

FIG. 2: (a) Electric field amplitude squared for the TE-like (top) and TM-like (bottom) supermode pairs of the directional coupler. (b) TE-like and TM-like transmission spectra for suspended channel WGs of varying widths, probed with a ≈ 1 μm FTW at room temperature. (c) Evolution of transmission minima with WG widths for the two polarizations in (c). Dashed lines are calculated phase-matching wavelengths for the fiber and WG. (d)-(f): Low temperature ($\approx$8 K) transmission and corresponding fiber-collected PL for WGs with increasing widths W_{ch}.

single FTW mode thus leads to efficient extraction of QD emission into the fiber. Detailed simulations have predicted a single QD collection efficiency as high as ≈ 35 % into an optical fiber (≈ 70 % including both fiber ends), with an operation bandwidth of tens of nm [11].

We first assessed the directional coupler without QDs, to confirm the basic light transfer mechanism between FTW and channel WG. A first set of suspended WGs with no QDs was fabricated on a 250 nm thick GaAs wafer for passive directional coupler characterization [12]. An ≈ 1 μm diameter FTW was brought into contact with individual channel WGs, forming directional couplers as illustrated in Fig. 1(c). Transmission spectra were obtained by launching broadband polarized light from a tungsten halogen lamp into the FTW input and analyzing output light with an optical spectrum analyzer. The FTW and channel WG each support a single guided mode of TE-like (x-oriented electric field) and TM-like (y-oriented electric field) polarizations. The resulting directional coupler supports a pair of hybrid supermodes for each polarization (Fig. 2(a)) [11]. The transmission spectrum for a given polarization is determined by the beating of the corresponding coupler supermodes, and exhibits minima when power is transferred from the FTW to the channel WG but not back into the FTW due to termination of the channel [12].

Several 8 μm long WGs with widths between 240 nm and 340 nm were measured. The transmission spectra (Fig. 2(b)) for the two main coupler polarizations displayed broad, $>$ 40 nm wide minima which typically reached $>$ 90 % extinction, evidencing efficient power transfer between the FTW and suspended WGs. After optical characterization, WG widths were measured with a scanning electron microscope. Figure 2(c) shows minimum transmission wavelengths as a function of WG width, along with the phase-matching wavelengths calculated with a vector finite element method [11]. The minima closely follow the calculated phase-matching wavelengths. The higher rate with which the TE-like phase-matching wavelength shifts with WG width is expected from these modes' higher intensity at the WG sidewalls. The agreement between theoretical and experimental curves indicates that the expected efficient directional coupler operation is indeed achieved.

We next attempted to validate efficient PL extraction from a second set of devices fabricated on a high QD density portion of the same wafer, where the QD ensemble s-shell emission peak was at $\approx$1200 nm. The QD-containing WGs were probed with a ≈ 1 μm diameter FTW in a cryostat at < 9 K temperature with the setup shown in Fig. S-3 of the supporting materials [12]. The devices were excited by launching a 50 MHz repetition rate, 50 ps width, 780 nm laser pulse train into the FTW. Figures 2(d)-(f) show TE polarization transmission and corresponding PL spectra for three devices of varying WG widths. PL collection over a range of a few tens of nm is achieved in all cases. The collected PL is maximized when the transmission dip - and thus the phase-matching wavelength - is aligned with the s-shell PL peak, evidencing efficient power transfer between phase-matched WGs. Fiber-collected PL of individual emission lines was typically 10 to 100 times higher than that obtained via free-space collection (from the same devices) with a 0.42 numerical aperture objective. Estimating the absolute collection efficiency was difficult, however, as the high density of QD lines prevented accurate determination of the intensity of any individual transition.

To avoid this difficulty, a third set of devices was fabricated with a low density of QDs, so that well-isolated transitions could be observed. These devices were produced from a 190 nm thick, GaAs WG layer wafer containing QDs with ensemble s-shell emission near 940 nm. Low-temperature PL spectroscopy was per-

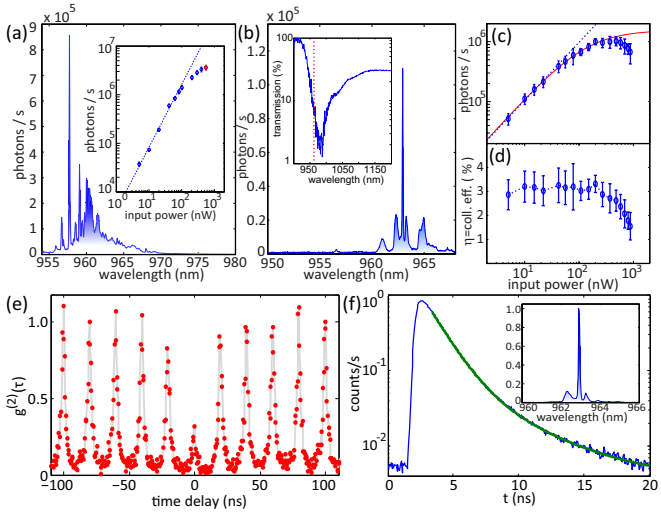

FIG. 3: (a)Fiber-collected single QD PL for the brightest device. Inset: photon rate for 957.7 nm line against pump power. (b) Fiber-collected single QD PL for second WG. Inset: directional coupler transmission spectrum, showing position of QD line. (c) Collected PL rate versus excitation power for 963 nm line in (b). Error bars are 95 % fit confidence intervals. Dashed line: linear fit to data below saturation. Continuous line: fit to theory. (d) Fiber collection efficiency obtained from (c), assuming ideal QD behavior. (e) Second-order correlation $g^{(2)}(\tau)$ and (f) lifetime for the excitonic line in (b), after a 1 nm bandpass filter (inset spectrum). Green line: bi-exponential fit.

formed as above, with a 50 MHz pulsed pump at 780 nm. Figure 3(a) shows the PL spectrum from the device that yielded the highest collection efficiency, for the sharp excitonic line at 957.7 nm. Driving this transition towards saturation (inset, Fig. 3(a)), at 550 nW pump power we estimate a collection efficiency into a single mode optical fiber $\eta = 6.05\ \% \pm 0.061\ \%$ [12]. We point out that the transmission of the collection portion of the FTW is $\approx 84\ \%$, so collection into the FTW (our first collection optic) is $7.250\ \% \pm 0.072\ \%$. The most likely reason for smaller collection efficiencies than predicted is non-optimal positioning of the QD in the GaAs WG, as supported by simulations presented in the supplementary material [12].

The 957.7 nm transition was located outside the operating wavelength band of the tunable bandpass filter available for spectral isolation, preventing further characterization of this device. A second WG was available, however, that displayed an isolated transition at ≈ 963 nm, shown in Fig. 3(b), located within the coupler transmission dip (inset). The evolution of the 963 nm peak collected PL rate into the single mode fiber as a function of pump power is shown in Fig. 3(c). For $P_{in} < 100$ nW, integrated PL counts increase linearly with pump power. A fit to the data assuming an ideal single exciton QD line (Fig. 3(c)) [12] matches the data for $P_{in} < 100$ nW, but overestimates the PL rate for $P_{in} > 100$ nW. For the highest measured PL intensity, the integrated counts correspond to $\eta \approx 2\ \%$. For $P_{in} \ll P_{sat} \approx 133$ nW, where the QD can be assumed to behave ideally, however, $\eta \approx 3\ \%$ (Fig. 3(d)).

To confirm the single photon nature of the 963 nm line of Fig. 3(b), we measured the second-order correlation, $g^{(2)}(\tau)$, for pulsed excitation at $P_{in} \approx 75$ nW (Fig. 3(e)). $g^{(2)}(0) = 0.29 \pm 0.02$ [12], indicating single QD emission that is dominantly comprised of single photons. The nonzero $g^{(2)}(0)$ is likely due to insufficient filtering, which allows uncorrelated photons and possible emission from other QDs to be detected. In particular, the spectrum of the detected light (inset in Fig. 3(f)) contains two broad sidelobes in addition to the 963 nm excitonic line. These may correspond to emission from other QDs with broadened lines, owing to proximity to WG sidewalls [13]. A bi-exponential decay of the excitonic line (Fig. 3(f)) with fast and slow lifetimes of 1.48 ns±0.08 ns and 4.6 ns±0.8 ns (uncertainties are 95 % fit confidence intervals) evidences non-ideal QD behavior. This is consistent with what is seen in $g^{(2)}(\tau)$ (Fig. 3(e)), where the coincidence counts between peaks do not return all the way to zero. The fast decay constant approaches the lifetime of a typical InAs QD (the lack of radiative rate enhancement is predicted in simulations [11]), while the long decay evidences QD coupling to nonradiative states that may lead to a reduced quantum efficiency and collection efficiency estimates.

In summary, we have demonstrated a fiber-coupled, QD single photon source based on a planar, guided wave nanophotonic coupler. We use this spectrally broadband approach to demonstrate an in-fiber, single QD PL collection efficiency of 6 %. Future work is aimed at improved efficiency through precise QD location [14, 15] within the device and understanding sources of non-ideal QD behavior.

Acknowledgments

This work was partly supported by the NIST-CNST/UMD-NanoCenter Cooperative Agreement. We thank R. Hoyt, C. S. Hellberg, Alexandre M.P.A. Silva, and Hugo Hernández-Figueroa for useful discussions.

[1] A. J. Shields, Nature Photonics **1**, 215 (2007), 0704.0403.
[2] H. Benisty, H. D. Neve, and C. Weisbuch, IEEE J. Quan. Elec. **34**, 1612 (1998).
[3] W. L. Barnes, G. Björk, J. Gérard, P. Jonsson, J. A. E. Wasey, P. T. Worthing, and V. Zwiller, Eur. Phys. J. D **18**, 197 (2002).

[4] G. Solomon, M. Pelton, and Y. Yamamoto, Phys. Rev. Lett. **86**, 3903 (2001).
[5] M. Pelton, C. Santori, J. Vuckovic, B. Zhang, G. S. Solomon, J. Plant, and Y. Yamamoto, Phys. Rev. Lett. **89**, 233602 (2002).
[6] S. Strauf, N. G. Stoltz, M. T. Rakher, L. A. Coldren, P. M. Petroff, and D. Bouwmeester, Nature Photonics **1**, 704 (2007).
[7] A. Muller, E. B. Flagg, M. Metcalfe, J. Lawall, and G. S. Solomon, Appl. Phys. Lett. **95**, 173101 (2009).
[8] V. Zwiller and G. Bjork, J. Appl. Phys. **92**, 660 (2002).
[9] A. N. Vamivakas, M. Atatüre, J. Dreiser, S. T. Yilmaz, A. Badolato, A. K. Swan, B. B. Goldberg, A. Imamoğlu, and M. S. Ünlü, Nano Letters **7**, 2892 (2007).
[10] J. Claudon, J. Bleuse, N. S. Malik, M. Bazin, P. Jaffrennou, N. Gregersen, C. Sauvan, P. Lalanne, and J. Gérard, Nature Photonics **4**, 174 (2010).
[11] M. Davanço and K. Srinivasan, Opt. Lett. **34**, 2542 (2009).
[12] See EPAPS supplemental material for additional experimental, simulation, and nanofabrication details.
[13] C. F. Wang, A. Badolato, I. Wilson-Rae, P. M. Petroff, E. Hu, J. Urayama, and A. Imamoglu, Appl. Phys. Lett. **85**, 3423 (2004).
[14] K. Hennessy, A. Badolato, M. Winger, D. Gerace, M. Atature, S. Guide, S. Falt, E. Hu, and A. Imamoglu, Nature (London) **445**, 896 (2007).
[15] S. M. Thon, M. T. Rakher, H. Kim, J. Gudat, W. T. M. Irvine, P. M. Petroff, and D. Bouwmeester, Appl. Phys. Lett. **94**, 111115 (2009).

Supplemental Information for Efficient quantum dot single photon extraction into an optical fiber using a nanophotonic directional coupler

M. Davanço,[1,2,*] M. T. Rakher,[1] W. Wegscheider,[3] D. Schuh,[3] A. Badolato,[4] and K. Srinivasan[1]

[1]*Center for Nanoscale Science and Technology, National Institute of Standards and Technology, Gaithersburg, MD 20899, USA*
[2]*Maryland NanoCenter, University of Maryland, College Park, MD 20742, USA*
[3]*Institute for Experimental and Applied Physics, University of Regensburg, D-93053 Regensburg, Germany*
[4]*Department of Physics and Astronomy, University of Rochester, Rochester, New York 14627, USA*

Finite difference time domain simulations

Finite difference time domain simulations were used to study the relationship between coupler transmission and PL spectra. The simulated structure consisted of a 1 μm diameter FTW of infinite extent and a 190 nm thick, 160 nm wide, 4 μm long GaAs channel waveguide. The computational domain was terminated with perfectly matched layers to simulate open boundaries.

Transmission spectrum

To determine the simulated transmission spectrum, a fundamental mode was launched into the FTW, at a 3 μm distance from the channel waveguide, and steady-state fields after the channel waveguide termination (for transmission) and before the mode launch position (for reflection), were recorded at various wavelengths. These fields were then convolved with the FTW mode and normalized to the injected power, to yield transmission and reflection spectra. Fig. S-1(a) shows transmission and reflection spectra for the structure with the above dimensions, and (b)-(d) show electric field profiles, recorded at the $x = 0$ plane, for FTW mode excitation at $z = -3$ μm at three different wavelengths. A broad transmission dip, and corresponding reflection peak, are observed in Fig. S-1(a) at $\lambda = 1072$ nm, where FTW and channel waveguide are phase-matched. In the corresponding field profile, Fig. S-1(c), it is evident that efficient power transfer occurs from the FTW into the waveguide, along the 4 μm extent of the latter. Due to waveguide termination at $z = 2$ μm, however, transfer back into the optical fiber is interrupted. Power guided in the channel is, instead, strongly scattered at the waveguide facet, and, as evidenced by the standing-wave pattern at $z < 0$, partially reflected back into the fiber. At wavelengths away from the phase-matching condition, Fig. S-1 (b) and (d), power launched into the fiber is transferred, without significant losses, past the GaAs guide, and transmission tends to 100 %, reflection to 0. Comparing the calculated transmission spectrum of Fig. S-1 to the measured curves in Fig. 2 in the main text, we see that the measured data matches prediction well in terms of their general shape and in particular, their depth and bandwidth.

PL spectrum

To determine simulated PL spectra, the structure was excited with a broadband electric dipole source, and the steady-state electromagnetic field at $z = 2$ μm was recorded for various wavelengths. These fields were convolved with the isolated FTW mode field as in ref. 1 to yield the fiber-coupled power. The total radiated power was also recorded, and was used to obtain the total collection efficiency. Figure S-2 shows collection efficiency for dipoles located at varying positions z_0 along the coupler length, with $z = 0$ at the center. Maximized collection collection is observed at wavelengths near 1050 nm, corresponding to the transmission dip in Fig. S-1, for $z_0 = -500$ nm. While efficient power transfer from the WG to the fiber occurs due to phase-matching, the coupler length must be long enough for sufficient transfer to occur, as evidenced by the considerably lower collection efficiencies obtained for the additional dipole positions simulated. For example, at $z_0 = 1500$ nm, the efficiency dips considerably below 10 % within the coupler operation band at $\lambda \approx 1050$ nm. The sensitivity of the extraction efficiency with dipole position along the coupler length is not surprising, given that it is in complete accordance with how a waveguide directional coupler is expected to operate. It does, however, represent a potential reason why theoretically-predicted efficiencies have not been achieved in experiment.

*Electronic address: mdavanco@nist.gov

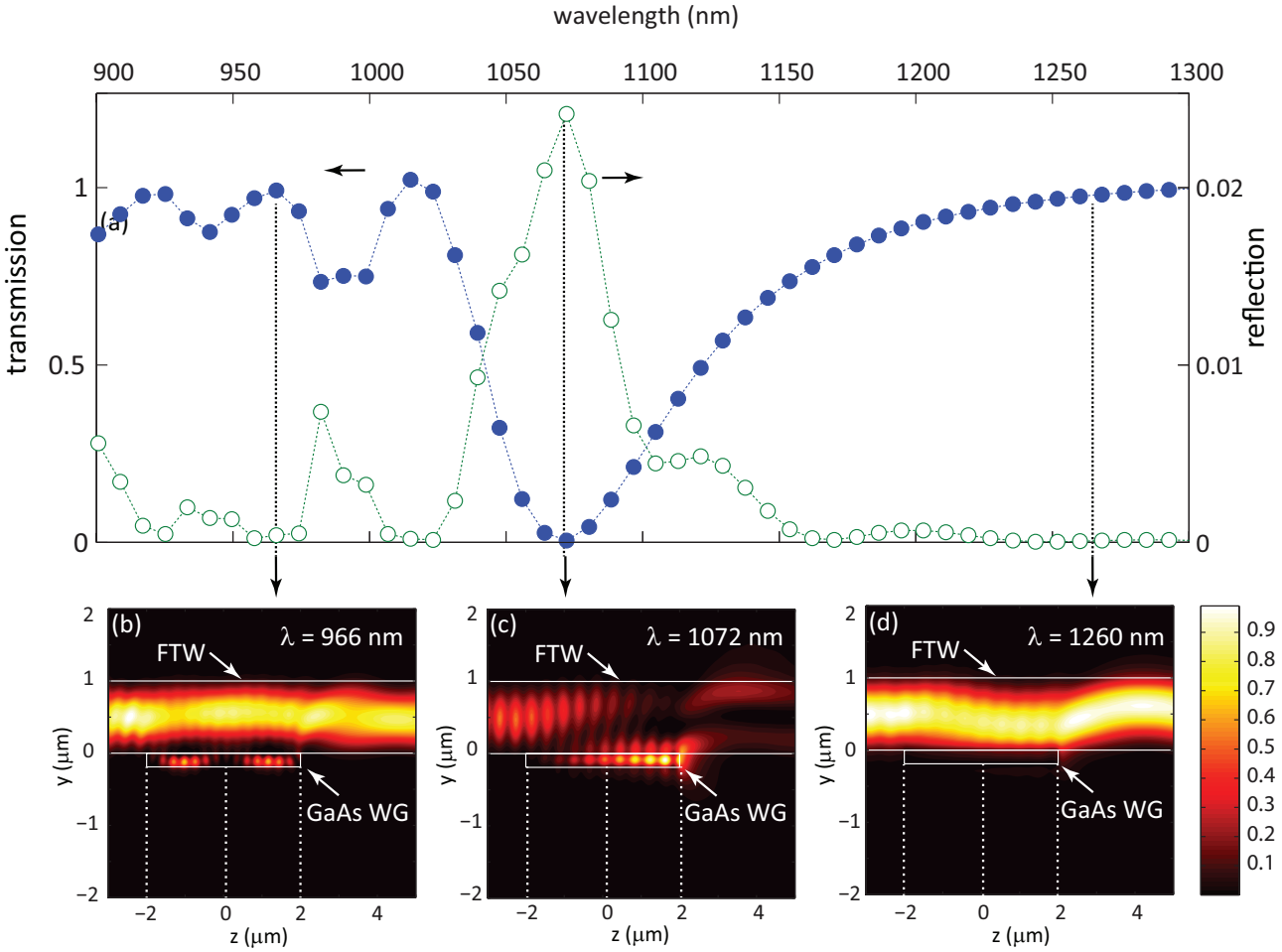

FIG. S-1: (a) Transmission (blue filled circles) and reflection (green open circles) spectra for simulated directional coupler formed by 1 μm diameter FTW and a 190 nm thick, 160 nm wide, 4 μm long suspended GaAs WG. (b)-(d) Steady-state, amplitude squared electric field at the $x = 0$ plane for fiber mode excitation at $z = -3$ μm at three different wavelengths. The coupler extends along the $\hat{z}$ direction, and the 4 μm long suspended GaAs WG is centered at $z = 0$.

PL extraction efficiency as a function of QD dipole orientation was studied numerically in ref. 2. The optimal dipole orientation is along the dominant polarization direction of the TE-like coupler supermodes, which is the $\hat{x}$-axis as defined in Fig. 1(a) in the main text. There, it was shown that if the dipole alignment was aligned along the $\hat{z}$-axis, the predicted PL extraction dropped by about a factor of 7. Thus, along with the QD's position, its dipole orientation may also reduce the measured collection efficiencies relative to the maximum possible values.

Experimental Details

Fabrication

Wafers were grown by molecular beam epitaxy, with an epistructure consisting of a GaAs waveguide layer on top of a 1 μm thick, $Al_xGa_{1-x}As$ ($x > 0.7$) sacrificial layer. Suspended GaAs WGs (Fig. 1(b) in the main text) containing self-assembled InAs QDs were fabricated using standard, submicron III-V processing techniques. Two different wafers were used, with waveguide layer thicknesses of 250 nm and 190 nm, and in the center of the waveguide a single layer of InAs QDs with a variable density gradient (from > 100 μm^{-2} to 0 μm^{-2}, along the $(01\bar{1})$ wafer direction) was grown, allowing for the creation of devices with varying QD densities.

Device fabrication was as follows. Electron-beam lithography with ZEP520-A resist was used to define waveguide patterns on top of a 200 nm SiN_x layer deposited on the epiwafer via plasma-enhanced chemical vapor deposition (PECVD). The patterns were transferred to the SiN_x through reactive ion etching (RIE) with a CHF_3/Ar mixture. Following resist removal, the waveg-

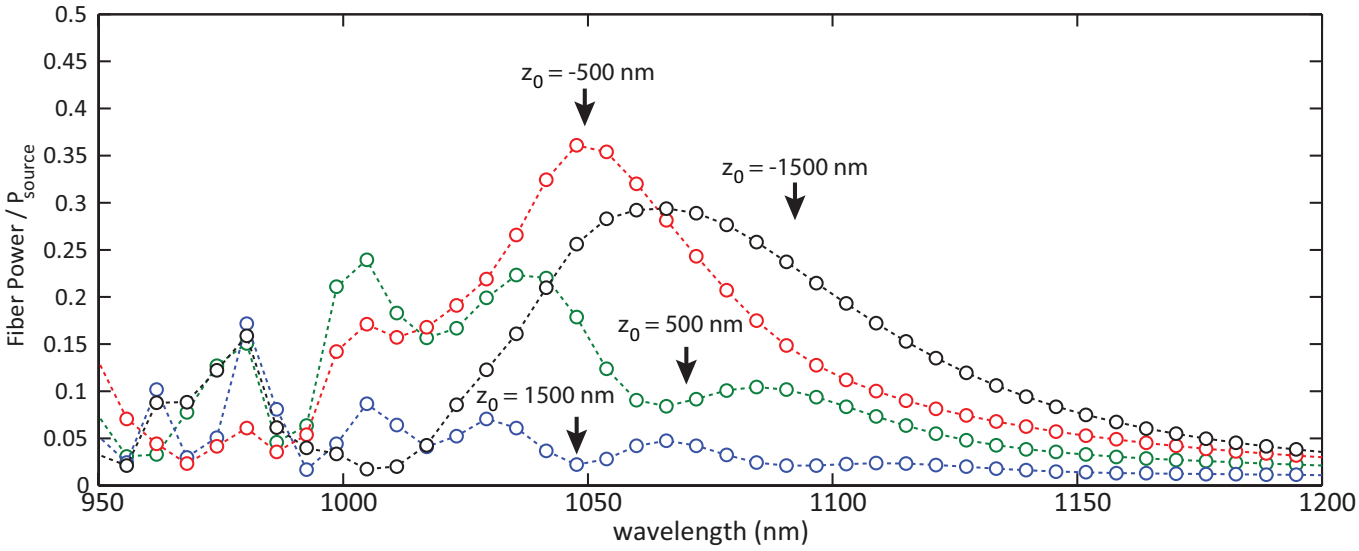

FIG. S-2: Predicted single QD photoluminescence collection efficiency into the optical fiber mode for the coupler from Fig. S-1. The curves were obtained by simulating a horizontally oriented electric dipole at the center of the channel waveguide cross-section ($x = 0$,$y = 0$), and at various positions z_0 along the longitudinal direction, $\hat{z}$ ($z = 0$ is at the center of the coupler, as in Fig. S-1).

uide patterns were transferred to GaAs through inductively coupled plasma (ICP) etching, with a Cl_2/Ar mixture. Finally, the sacrificial layer and remaining SiN mask were removed with a $>$ 10 s, 49 % HF dip. In many devices, the SiN_x mask layer was omitted and direct transfer from the electron-beam mask to the GaAs was performed using the same ICP etch. No significant change in device quality or performance was observed in going from a straight electron-beam mask to a SiN_x mask.

For device interrogation within the cryostat, it was often most convenient to isolate the waveguide devices to a mesa that was $\approx$15 μm above the rest of the sample's surface. This was done through contact photolithography and a H_2O_2:H_3PO_4:CH_3OH (10:1:1 by volume) solution at 50 °C for 30 min.

The material containing dots with s-shell emission near 940 nm was annealed in a rapid thermal annealer at $\approx$ 830°C for 30 s prior to fabrication. This was done to blue-shift the QD s-shell emission, which originally occurred at $\approx$ 1100 nm. In addition, a first set of measurements revealed that fabricated waveguides were insufficiently narrow to achieve phase-matching to the FTW in a wavelength-band matching the QD emission. To rectify this, a digital GaAs wet etch technique[3] was employed to reduce the waveguide dimensions appropriately. The process consisted of alternately oxidizing the GaAs in H_2O_2 and removing the formed oxide layer with a 1 molar solution of citric acid ($C_6H_8O_7$).

Transmission spectrum measurement

As illustrated in Fig. 1 in the main text, a FTW of $\approx$ 1 μm diameter was brought into contact with individual waveguides, forming directional coupler structures that are interrogated using the experimental setup depicted in Fig. S-3. Light from a quartz-tungsten-halogen lamp was coupled into a single-mode optical fiber and passed through an in-line polarizer and polarization controller, and then launched into the FTW input. An optical spectrum analyzer (OSA) was used to obtain transmission spectra, from 1100 nm to 1600 nm, for the formed directional couplers. To obtain spectra for the two main polarizations, the polarization controller was used to minimize transmission at some wavelength range after the WGs were first put in contact. This range was assumed to be that for which power transfer from the suspended WG to the fiber was maximized, for one of the two main polarizations. A spectrum was recorded, the fiber lifted and a background spectrum was then taken. The fiber was next brought back in contact with the GaAs guide, and a second spectrum was taken to verify that the transmission minima, and thus the polarization, was unchanged. The polarization controller was next used to maximize the transmission at the minimum wavelength range, and a second transmission spectrum was taken, assumed to be for the second main polarization. Finally, the fiber was lifted and a second background spectrum was recorded.

The minimum transmission wavelengths plotted on Fig. 2(b) in the main text correspond to measured global transmission minima. Detection noise leads to uncertainties in the determination of an actual minimum transmission wavelength. This is represented by error bars in the figure, which correspond to intervals over which the transmitted power fluctuates below 1.05 times the minimum transmission.

To determine the waveguide widths, top view scanning electron microscope images of the devices were taken, and an edge

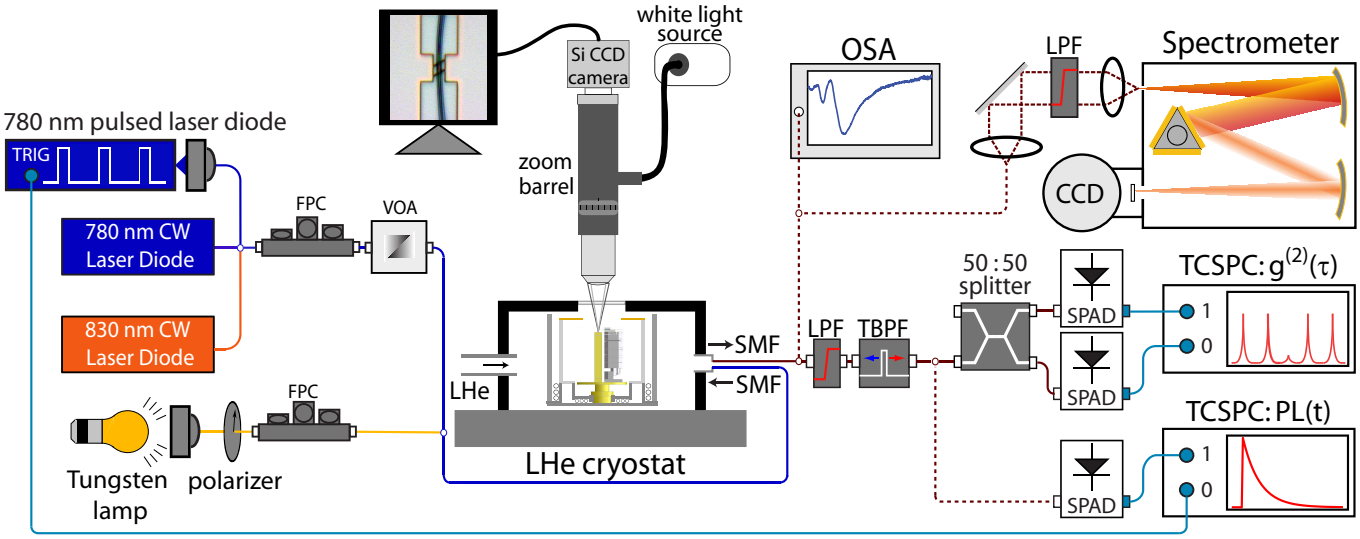

FIG. S-3: Experimental setup for cryogenic transmission and photoluminescence measurements. VOA: variable optical attenuator; SMF: single mode optical fiber OSA: optical spectrum analyzer; LPF: long wavelength pass filter; TBPF: tunable bandpass filter; FPC: fiber polarization controller; SPAD: single photon avalanche detector; TCSPC: time correlated single photon counter; CCD: charge-coupled device; LHe: liquid helium; TRIG: trigger.

detection technique was employed to determine sidewall profiles along the waveguide length. For each waveguide, averages and standard deviations were obtained for the locations of the two waveguide sidewalls, which were then used to calculate waveguide widths and corresponding deviations due to sidewall roughness. The standard deviations are plotted as error bars in the graph of minimum transmission wavelength versus waveguide width on Fig. 2(b) in the main text.

Determination of collection efficiency

Collected photon rates were determined from PL spectra, after calibration of Si CCD count rates against the known optical power of a (fiber-coupled) continuous wave laser source, tuned to the QD emission wavelength. Integrated counts in the spectrum of a 100 fW laser signal led to a conversion factor of 130 photons/CCD count. We point out that this conversion factor, which includes the spectrometer in-coupling efficiency, grating efficiency, and CCD detection efficiency and gain, falls within the expected range, considering manufacturer-provided specifications. The Si CCD quantum efficiency is < 10 % at 960 nm, the CCD gain was set to 3 photoelectrons/CCD count, and the grating efficiency is around 50 %.

When measuring PL, a long-wavelength pass filter at 850 nm was introduced before the spectrometer slit, with a nominal transmission of 80 %. With this, the collected photon rate into the single mode fiber was calculated as $R_{ph.} = R_{det.} \cdot 130/0.8$. To determine the emitted photon rate, the QDs were pumped into saturation and assumed to have 100 % radiative efficiency. Under these conditions, the emission rate is that of the pump source, 50 MHz. The collection efficiency into the single mode fiber, η, is then given as $\eta = R_{ph.}/50\times10^6$.

Considering an ideal single exciton QD line, the collected photon rate R_{ph} is given by the product of the collection efficiency η, the pulse repetition rate $R_{rep.} = 50$ MHz and the average exciton occupancy per pulse: $R_{ph} = \eta \cdot R_{rep}/(1 + P_{in}/P_{sat})$, where P_{in} is the average pump power and P_{sat} is the pump saturation power. This model fits the data of Fig. 3(c) reasonably well for $P_{in} < 100$ nW, with $P_{sat} = 133.2$ nW$\pm$21.7 nW (the uncertainty is a 95 % fit confidence interval, associated with errors in the determination of the emission rates of the isolated excitonic line). For $P_{in} > 100$ nW, however, it overestimates the output PL rate, and for $P_{in} > 580$ nW, a marked decline in PL intensity is observed, suggesting that the emission rate starts to decrease before QD saturation is achieved.

$g^{(2)}(\tau)$ measurements

A fiber-based Hanbury-Brown and Twiss configuration was used to obtain the second-order correlation curve shown in Fig. 3(e) in the main text. The excitation was pulsed and below saturation ($P_{in} \approx 75$ nW). The setup consisted of two Si single photon avalanche detectors (SPADs) connected to the output ports of a 3dB optical fiber splitter, and a time-correlated single photon counting instrument, which performed histogramming of the photon arrival time differences. The SPAD detection

efficiency was determined to be 26 % ± 4 % and the splitter transmission 37 % ± 1 % per arm. The PL signal from the FTW was filtered with a fiber coupled, 900 nm long-wavelength pass filter, followed by a fiber coupled, tunable, thin-film filter with a 1 nm bandwidth, with a 55 % ± 4 % transmission. The total transmission through the two filters was 26 % ± 2 %.

To obtain the $g^{(2)}(0)$ value quoted in the text, we integrated the peaks in Fig. 3(e) in the main text over increasing intervals up to half the repetition period, and calculated averages. The mean and standard deviation values for the zero time peak (which corresponds to $g^{(2)}(0)$) were then normalized by an average of all other integrated (averaged) peak values.

To estimate the percentage of background emission in the analyzed signal, we derived an expression for $g^{(2)}(\tau)$ for the case of detection of QD emission together with perfectly uncorrelated background light. The second order correlation function for the total detected light is

$$g^{(2)}(\tau) = \frac{\langle I(t)I(t+\tau)\rangle}{\bar{I}^2}, \tag{S-1}$$

where $I(t) = I_{QD}(t) + I_{bg}(t)$ is the total detected intensity, I_{QD} and I_{bg} are the quantum dot emission and background intensities respectively, and $\bar{I} = \langle I(t)\rangle$. Assuming

$$\langle I_{QD}(t)I_{bg}(t+\tau)\rangle = \langle I_{bg}(t+\tau)I_{QD}(t)\rangle = \bar{I}_{QD}\bar{I}_{bg}, \tag{S-2}$$

we get

$$g^{(2)}(\tau) = \frac{\left(\bar{I}^2 - \bar{I}_{QD}^2\right) + \bar{I}_{QD}^2 \cdot g_{QD}^{(2)}(\tau)}{\bar{I}^2}, \tag{S-3}$$

with $g_{QD}^{(2)}(\tau) = \langle I_{QD}(t)I_{QD}(t+\tau)\rangle$. From this expression, the zero-time second-order correlation for the QD alone is

$$g_{QD}^{(2)}(0) = 1 + \left(\frac{1+R}{R}\right)^2 \cdot [g^{(2)}(0) - 1], \tag{S-4}$$

where $g^{(2)}(0)$ is the measured quantity, and $R = I_{QD}/I_{bg}$ is the ratio of QD light intensity I_{QD} over background light intensity I_{bg} at the detector (i.e., R is the signal-to-background ratio). Since $I_{QD} + I_{bg} = I$, we get

$$\frac{I_{bg}}{I_{total}} = \frac{1}{1+R}. \tag{S-5}$$

Assuming perfectly antibunched single QD emission, R was obtained by setting $g_{QD}^{(2)}(0) = 0$, and the background ratio over the total was computed from S-5.

Assuming that the detected signal is composed of perfectly antibunched light from the single QD emission peak at 963 nm and uncorrelated background photons, we determine that 16 % of the total detected photons would correspond to background emission. In this case, since the area under the sharp excitonic line in the spectrum of the main text's Fig. 3(e) inset is ≈ 51 % of the total, the broad features would have to be produced in part by the same QD. A more likely situation is that the detected signal also includes emission from additional (broadened) QDs.

Photoluminescence excitation spectroscopy

In addition to photoluminescence spectroscopy, our fiber-based technique can be used for photoluminescence excitation (PLE) spectroscopy of single quantum dots, even in samples with a high density of emitters. In such a measurement, the QD is excited quasi-resonantly in the p-shell, by a continuous wave, tunable external cavity diode laser (ECDL), and the s-shell PL is recorded as the excitation wavelength is scanned. This type of measurement has been used in the past to reveal carrier scattering mechanisms leading to s-shell photon emission[4,5].

We next describe a single QD PLE measurement performed on a high QD density sample, with s-shell emission near 1000 nm, as shown in the inset of Fig. S-5 (a). In our experimental setup, Fig. S-4, the QD was excited with continuous wave light from a 963 nm to 995 nm ECDL via the FTW. The emitted s-shell PL, collected back into the input fiber (i.e., flowing in the direction opposite to that of the excitation light), was diverted towards a grating spectrometer through a 10:90 directional fiber coupler. This was done to reduce the intensity of excitation light at the spectrometer entrance, which would otherwise have overwhelmed the PL signal. The laser wavelength was set to be scanned over a portion of the QD ensemble p-shell range, with a rate of 10 pm/s. During the scan, photoluminescence spectra with a 1 s integration time were continuously recorded.

Figure S-5(a) shows fiber collected s-shell emission for an excitation wavelength $\lambda_{in} = 963.4$ nm, for which a bright, single QD line at $\lambda = 990.5$ nm becomes visible. The evolution of this line's intensity for λ_{in} varying between 961.5 nm and 965 nm

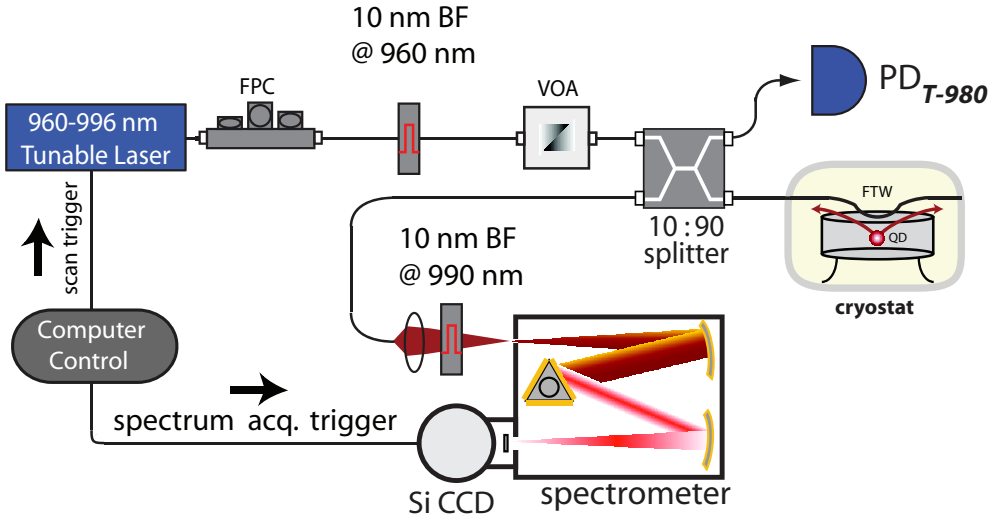

FIG. S-4: Photoluminescence excitation spectroscopy setup

is shown Fig. S-5(b), with a spectral resolution better than 30 pm. The excitation spectrum displays sharp peaks related to the carrier dynamics leading to s-shell emission[4,5].

To confirm that the selected PL line is indeed produced by single dot, photon correlation measurements are performed with a Hanbury-Brown and Twiss setup, for $\lambda_{in} = 963.4$ nm. A 1 nm, fiber-based tunable bandpass filter was used to filter the PL signal. The antibunching dip at zero delay ($g^{(2)}(0) \approx 0.5$) shown in Fig. S-5(c) confirms that the p-shell excitation through the coupler can indeed select a single QD from within the dense ensemble. The nonzero antibunching is most likely due to the limited measurement resolution (256 ps) and insufficient bandpass filtering, especially considering the high QD density of the sample. Bunching peaks surrounding the antibunching dip are also observed (Fig. S-5(d)), with a decay time of a few hundreds of nanoseconds, and are possibly related to the formation of charged QD states[6].

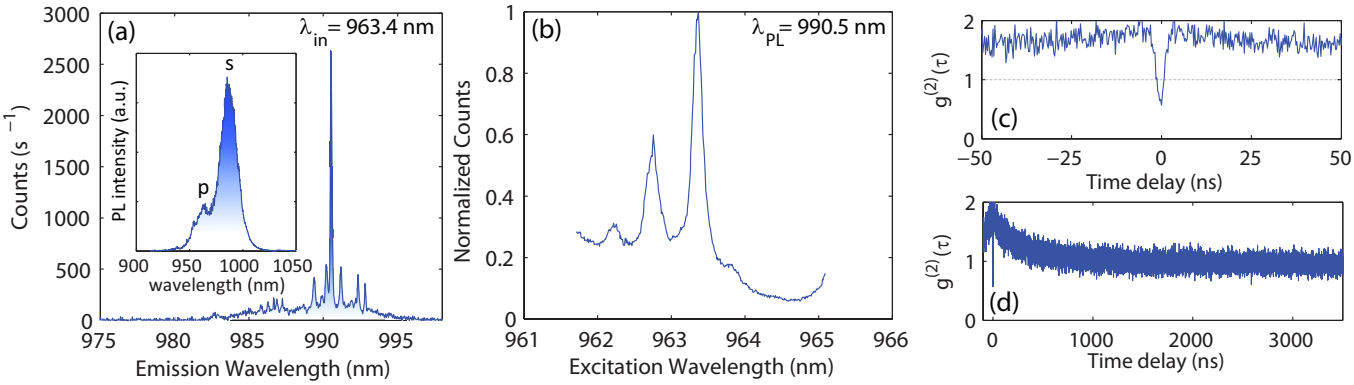

FIG. S-5: (a) Fiber-collected PL spectrum for CW quasi-resonant excitation at $\lambda = 963.4$ nm. Inset: ensemble QD non-resonant PL spectrum, obtained via free-space collection. (b) Evolution of PL intensity for the single dot at $\lambda = 990.5$ nm, for varying excitation wavelengths. (c) CW second-order photon correlation trace for the PL peak at $\lambda = 990.5$ nm in (a). (d) same as (c), with longer time span.

1 M. Davanço and K. Srinivasan, Opt. Express **17**, 10542 (2009).
2 M. Davanço and K. Srinivasan, Opt. Lett. **34**, 2542 (2009).
3 K. Hennessy, A. Badolato, A. Tamboli, P. M. Petroff, E. Hu, M. Atature, J. Dreiser, and A. Imamoglu, Appl. Phys. Lett. **87**, 021108 (2005).
4 Y. Toda, O. Moriwaki, M. Nishioka, and Y. Arakawa, Phys. Rev. Lett. **82**, 4114 (1999).
5 T. Warming, E. Siebert, A. Schliwa, E. Stock, R. Zimmermann, and D. Bimberg, Phys. Rev. B **79**, 125316 (2009).
6 C. Santori, D. Fattal, J. Vuckovic, , G. S. Solomon, E. Waks, and Y. Yamamoto, Phys. Rev. B **69**, 205324 (2004).